

# Segmentation and Analysis of Nerve Fibers in Histologic Sections of the Cerebral Human Cortex

Maren Pakura<sup>1</sup>, Oliver Schmitt<sup>2</sup>, Til Aach<sup>1</sup>

<sup>1</sup> Institute for Signal Processing, Medical University of Lübeck

<sup>2</sup> Institute for Anatomy, Medical University of Lübeck

Ratzeburger Allee 160, D-23538 Lübeck, Germany

E-mail: pakura@informatik.mu-luebeck.de, schmitt@anat.mu-luebeck.de,  
aach@isip.mu-luebeck.de

## Abstract

*This paper describes an image acquisition and processing chain toward the analysis of images of thin histologic sections of the cerebral human cortex. We are particularly interested in the spatial distributions of nerve fibers, the inhomogeneities of which indicate architectonic and functional changes between different cortical areas. We therefore focus on the development of a specific optical and algorithmic chain to acquire histologic images in an appropriate resolution, and to enhance, segment, skeletonize and separate nerve fibers in these images. The processing results prepare the images for subsequent local measurements of nerve fiber orientation, fiber lengths, fiber density, area fraction occupied by fibers, and others.*

## 1. Introduction

This paper deals with the acquisition and processing of images of thin histologic sections of the human cerebral cortex. In different regions of interest (ROIs) of such images, the nerve fibers may be homogeneously or inhomogeneously distributed. Inhomogeneities of the spatial distribution in adjacent cortical areas are indicators of architectonic changes (transitions) which correlate with functional changes. To allow the detection of such changes, the nerve fibers in the sections are first selectively stained to increase their contrast in the acquired images. Changes of their distribution properties, however, cannot always be detected by a human observer without quantification [6]. Earlier, such quantification algorithms were developed for histologic images of cell profiles [10], where the volume fraction occupied by cell profiles was locally estimated. For nerve fiber analysis, however, this quantification approach is only partly sufficient because nerve fibers are much thinner and

possess a geometry and morphology very different from those of the cell bodies in [10]. Therefore, we focus here on an image processing chain which enhances, segments, skeletonizes and separates nerve fibers. Based on processed versions of an input image at the various stages of our processing chain, distribution features like nerve fiber density, nerve fiber lengths, area fraction occupied by fibers, fiber orientation, and others can locally be measured.

## 2. Image acquisition

The images are acquired from thin histologic sections of the cerebral human cortex by a video microscope (AxioPhot microscope and AxioCam scanner camera, Zeiss Vision). Before acquisition, the nerve fibers are stained. (In detail,  $20\mu\text{m}$  thick histologic sections were stained for 24 hrs in a 0.1% silver nitrate borax buffered solution followed by development in 1% gold chloride, 2% oxalic acid and 5% sodium thiosulphate. The stained sections were dehydrated and mounted with Entellan.) The position of the histologic section relative to the video microscope is controlled along three orthogonal axes by motors. The motors of the  $x$ - $y$ -plane shift an observer-defined ROI of the histologic section meander-like through the field of view of the microscope, which captures and digitizes the ROI in a mosaic-like manner. After each shift, the field of view is recorded as an 8-bit grey-level image of  $512 \times 512$  pixels. By measurements, we verified that each pixel of the acquired images corresponds to an area of  $0.503 \times 0.503\mu\text{m}^2$  of the histologic section, what proved to be well suited for computerized analysis of neurons and nerve fibers. On the screen, the images appear with a size of  $170 \times 170\text{mm}^2$ . For the given screen, this magnification by a factor of 660 is determined by the object lens, which contributes a factor of 20, by an additional lens (Optovar) positioned between object lens and camera contributing a factor of 1.25, and finally by the projection

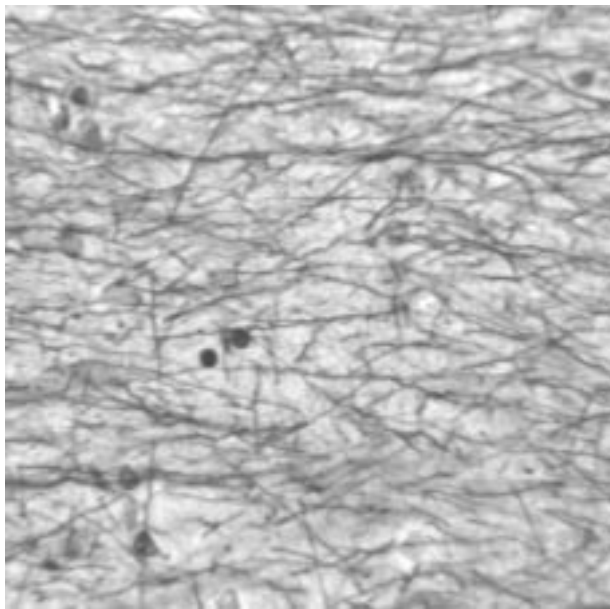


**Figure 1.** Tile of size  $512 \times 512$  pixels of a histologic section image.

geometry, which results in an another factor of 26.4. As shown in Fig. 1, the nerve fibers appear as a web of dark elongated structures in these images. The dark blobs also visible in Fig. 1 are cell nuclei, which must be eliminated for nerve fiber analysis.

### 3 Image processing

#### 3.1. The Processing Chain

The purpose of our algorithms is to provide information about the nerve fibers at different levels of abstraction. The full chain is shown in Fig. 2. First, the stained fibers are enhanced relative to other structures, while simultaneously large cell nuclei are removed. The enhanced fibers can then rather reliably be segmented by a thresholding algorithm. In the resulting binarized image, nerve fibers are represented by black lines of corresponding widths. The final step is to separate and disentangle the fibers by skeletonization. Since the mosaicked images of the histologic sections may be very large (a full image of a section of about  $7 \times 2.8 \text{mm}^2$  consists of  $27 \times 11$  tiles of  $512 \times 512$  pixels each) the processing is applied to each tile individually, with overlap where appropriate.

#### 3.2. Nerve fiber enhancement

In the grey level images, the stained nerve fibers appear as dark and narrow objects. A well suited approach to en-



**Figure 2.** Diagram of the image processing chain.

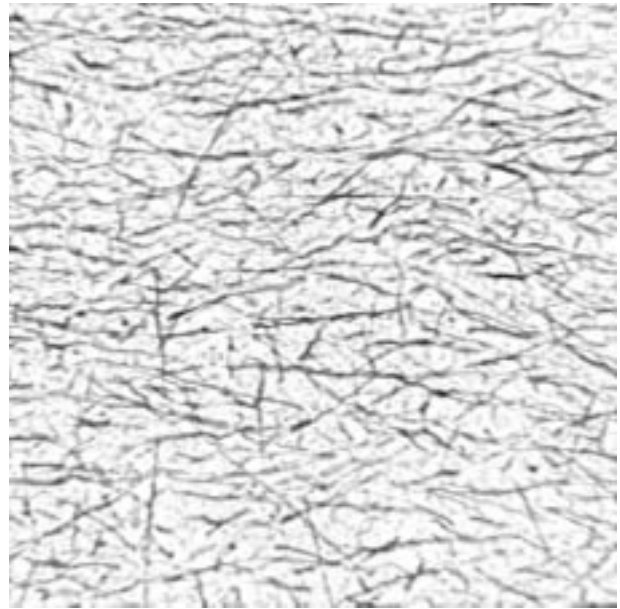


**Figure 3.** External tophat transform of Fig. 1.

hance these is the external top-hat transform [4, 8]. This transform of an image is defined as the difference between the morphological closing of the image and the image itself. We used a binary square window of  $9 \times 9$  pixels as structuring element. The closing is then realised by a maximum operator followed by a minimum operator inside a  $9 \times 9$ -pixel sliding window, which corresponds to a size of  $4.5 \times 4.5 \mu\text{m}^2$ . This is larger than the diameter of the nerve fibers, but smaller than the cell nuclei. The sliding maximum operator thus removes the fibers, while the sliding minimum restores background structures — including the cell nuclei which are not completely removed by the maximum — affected by the maximum operator. For computational simplicity, both the maximum and minimum operator are realized in a separable manner by 1D-masks applied successively along rows and columns. The difference image then mainly contains fibers. A top-hat filtered result is shown in Fig. 3.

#### 3.3. Nerve fiber segmentation

In the tophat-transformed images, the stained nerve fibers are generally dark against a mainly bright background, so that segmentation by thresholding appears feasible. To find the threshold, we seek a parameterless and un-

supervised method. These criteria are met by Otsu’s threshold selection method [9]. The method first calculates the normalized grey level histogram of the tophat transformed image. Thresholding can then be viewed as an unsupervised classification problem into the two classes “fibers” and “background”. The classes are described by their class mean values, class variances and class prior probabilities. Any given threshold divides the histogram into two clusters, from which these quantities are estimated. The threshold is selected such that measures of class separability are maximized. Three equivalent such measures are discussed in [9]. In the end, the threshold is determined such that the sum of the in-class variances weighted by their estimated class prior probabilities is minimized. This is identical to maximizing the between-class variance, defined as the squared distance between the two class means weighted by the class prior probabilities. Note that the class prior probabilities indicate the fractions occupied by fibers and background, respectively, in the analyzed image.

We apply the thresholding approach to each mosaic tile of  $512 \times 512$  pixels individually. To enforce some coherence between neighbouring thresholds, the normalized histograms are actually calculated from overlapping regions of size  $600 \times 600$  pixels. Furthermore, the signed tophat transformed images are first rescaled to 0-255 by an affine transform. The class separability measures in [9] are invariant to such an operation. (Indeed, in [9] the weighted sum of the in-class variances is normalized by the total image variance, which is independent of the threshold, to achieve this invariance.) The segmentation result is a binary image where the nerve fibers are represented by black lines of corresponding widths (Fig. 4).

### 3.4. Nerve fiber skeletonization

From the segmented nerve fibers, quantities like area fraction occupied by the fibers and similar measures can already be locally computed. Other measures require counts of nerve fibers, which first need to be separated. To separate the nerve fiber lines, it is advantageous to convert each line into its skeleton. Hence, the next step is to skeletonize the fiber segments [7, 2]. The purpose of skeletonization is to thin the fiber segments to lines one pixel wide. These lines should be approximately in the middle of the original segments rather than close to segment edges. Also, the skeletonization algorithm should preserve intersections of fiber segments. Moreover, skeletonization should preserve single segments, i.e. a segment must not be separated into non-connected lines.

To thin segments, the skeletonization algorithm removes object pixels subject to the criterion that doing so does not lead to a fragmentation of the object. To obtain skeleton lines which correspond roughly to the middle axes of the

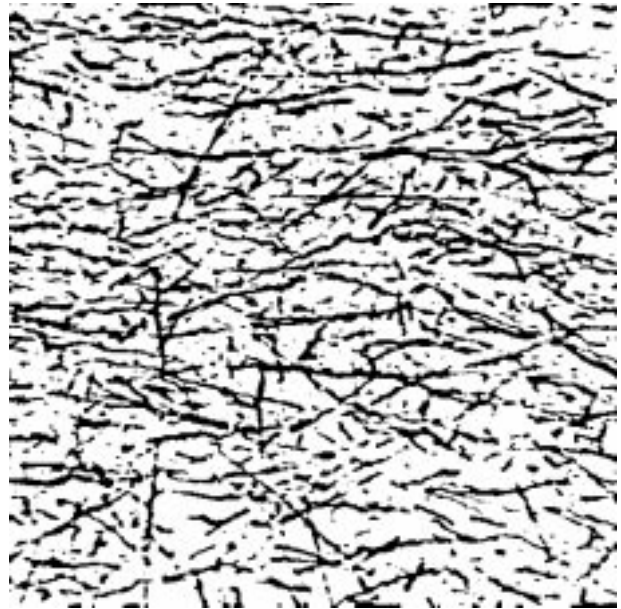


**Figure 4.** Segmentation result for Fig. 1, obtained by thresholding its tophat transformed version in Fig. 3.

fiber segments, object pixels are removed iteratively from the different object edges (north, south, east, west) by repeatedly scanning the image matrix. For each object edge, the conditions which permit to remove an object pixel [1] can rather compactly be expressed [11] using the features “connectivity number” and “crossing number” [12]. For the implementation, these conditions can be captured by binary patterns in the  $3 \times 3$ -neighbourhood of a tested pixel [2]. These patterns are shown in table 1.

For each object edge pixel, the algorithm compares the  $3 \times 3$ -neighbourhood to these patterns, depending on whether the pixel is located at a north, south, east or west

**Table 1.** Test pattern set for the north, south, east and west edges of binary objects. Here, object pixels are indicated by ones, and background pixels by zeros. The pixels labelled by X may take either the value one or the value zero.

North			South			East			West		
1	1	1	0	0	X	1	X	0	X	X	1
X	P	X	X	P	X	1	P	0	0	P	1
X	0	0	1	1	1	1	X	X	0	X	1
X	1	1	X	0	X	1	1	X	X	0	X
0	P	1	1	P	0	1	P	0	0	P	1
X	0	X	1	1	X	X	0	X	X	1	1



**Figure 5.** Skeleton of Fig. 4.

edge. The object edge pixel is removed from the object (i.e. it is relabelled as a background pixel) if its  $3 \times 3$ -neighbourhood is found to be identical to one of the test patterns. These iterations are repeated until a stable skeleton is reached.

Fig. 5 shows the skeleton obtained from the segmentation in Fig. 4. To allow a better visual assessment of the extracted nerve fibers, the skeleton is shown in Fig. 6 together with the original in Fig. 1. In a similar manner as for segmentation, skeletonization is applied separately to each mosaic tile of size  $512 \times 512$  pixels, with a small overlap between the segmentations of neighbouring tiles.

The described skeletonization algorithm preserves bifurcations and intersections. Such bifurcations and intersections are, however, often caused by projective overlap of fibers in different depths of the histologic section. Based on the skeleton, we have implemented three different options to separate different nerve fibers:

- The bifurcations and intersections of the skeleton are assumed to correspond to true fiber branchings in the histologic section, and are thus kept unchanged.
- Bifurcations with a small angle between the two branches are assumed to represent true nerve branching, while those with larger angles are regarded as resulting from projective overlap. In this option, branchings with angle between 70 degrees and 90 degrees are decomposed into two non-connected fibers.
- All bifurcations and intersections of the skeleton are regarded as stemming from projective overlaps, and

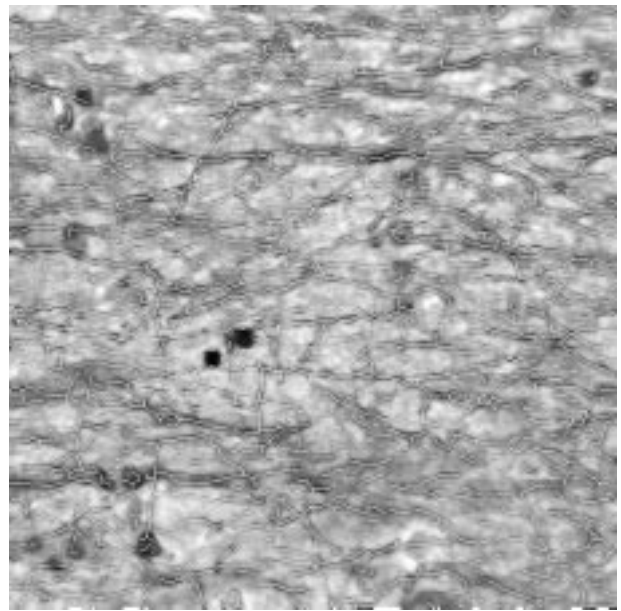


**Figure 6.** Skeleton of Fig. 5 overlaid over the original in Fig. 1.

are thus decomposed into their individual branches.

### 3.5. Postprocessing of the skeleton

The resulting skeletons are generally not yet error-free. Firstly, as can be gathered from Fig. 6, there may occur very short erroneous lines which do not correspond to nerve fibers. These errors can be caused by spurious regions falsely detected by the segmentation algorithm. Furthermore, thick lines with outgrowths in their edges may create false branchings. We therefore remove all lines shorter than 14 pixels, corresponding to a distance of about  $7\mu m$  or less in the histologic section. The result of this operation is shown in Fig. 7.

The second problem in the skeleton images are occasional circular structures which do not exist in real neuronal tissues. These artifacts are caused by the projective overlap of several nerve fibers distributed in the depth of the thin tissue sections. We separate these using the the flood-fill algorithm in Foley [5]. The algorithm starts by flooding the skeletonized image from its edges, viewing the skeletonized fibers as dams. Small areas which remain “dry” lie within such circular structures. After checking for additional dams inside each detected circular structure undesired circles are resolved by first converting the area inside the circles to fiber segments, which are subsequently skeletonized. The algorithm is straightforward and highly recursive. The recursivity, however, led to stack overflows. Instead of processing the whole stack, the algorithm is therefore imple-



**Figure 7.** Skeleton of Fig. 5 after removal of lines shorter than 14 pixels.



**Figure 8.** Skeleton of Fig. 7 after application of the flood/fill algorithm.

mented with a vector container. The result is shown in Fig. 8. Evidently, circular structures have been removed. Since this algorithm, however, displaces the remaining skeleton lines, it should be applied with caution.

## 4 Conclusions

We have presented an image processing chain which allows to enhance, segment, skeletonize and disentangle nerve fibers in images of histologic sections acquired by a video microscope. The different stages of our processing chain prepare the images for analysis of fiber density, fiber orientation, fiber lengths and others. We currently work on two improvements of this chain: firstly, we seek increase the segmentation performance by combining Otsu's threshold selection with a two-threshold procedure, similar as applied in the Canny edge detector [3]. Secondly, we seek to resolve closed loops in the skeleton by a less severe alternative to the flood/fill algorithm. Future work will then be directed toward analysis of nerve fiber distributions in the processed images.

## References

- [1] C. Arcelli. A condition for digital points removal. *Signal Processing*, 1:283–285, 1979.
- [2] C. Arcelli, L. Cordella, S. Levisaldi. More about a thinning problem. *Electronics Letters*, 16:51–53, 1980.

- [3] J. Canny. A computational approach to edge detection. *IEEE T PAMI*8:679–698, 1986.
- [4] E. R. Dougherty. *Mathematical Morphology in Image Processing*. Marcel Dekker, New York, 1992.
- [5] J. D. Foley et al. *Computer Graphics: Principles and Practice*. Addison-Wesley, Reading, Mass., 1996.
- [6] S. Geyer et al. Two different areas within the primary motor cortex of man. *Nature*, 382:805–807, 1996.
- [7] R. Klette, P. Zamperoni. *Handbook of Image Processing Operators*. John Wiley, Chichester, 1996.
- [8] V. H. Metzler. *Morphologische Dekomposition als universelle Methodik der medizinischen Bildverarbeitung: Grundlagen und praktische Umsetzung*. Dissertation, Universität Lübeck, 2002.
- [9] N. Otsu. A threshold selection method from gray-level histograms. *IEEE T SMC*9(1):62–66, 1979.
- [10] A. Schleicher, K. Zilles. A quantitative approach to cytoarchitectonics: Analysis of structural inhomogeneities in nervous tissue using an image analyzer. *J Microsc*157:367–381, 1990.
- [11] H. Tamura. A comparison of line thinning algorithms from digital geometry viewpoint. In *Proc. 4th ICPR*, 715–719, Kyoto, 1978.
- [12] S. Yokoi, J. I. Toriwaki, T. Fukumura. An analysis of topological of digitized binary pictures using local features. *CGIP*4:63–73, 1975.